ISSN 1063-780X, Plasma Physics Reports, 2022, Vol. 48, No. 4, pp. 327–336. © The Author(s), 2022. This article is an open access publication.
Russian Text © The Author(s), 2022, published in Fizika Plazmy, 2022, Vol. 48, No. 4, pp. 306–316.

PLASMA–WAVE INTERACTION

Methods for Reducing Anomalous Losses in ECRH Experiments at Second Resonance Harmonic

E. Z. Gusakov[a], * and A. Yu. Popov[a], **

[a] *Ioffe Institute of the Russian Academy of Sciences, Saint Petersburg, 194021 Russia*

**e-mail: evgeniy.gusakov@mail.ioffe.ru*

***e-mail: a.popov@mail.ioffe.ru*

Received November 30, 2021; revised December 19, 2021; accepted December 25, 2021

Abstract—An approach is analyzed that makes it possible to reduce anomalous absorption in experiments on electron cyclotron resonance heating (ECRH) at the second harmonic of the electron cyclotron resonance. The anomalous absorption is associated with excitation of the low-threshold parametric decay instability of the extraordinary pump wave at the local maximum of the nonmonotonic density profile. The general case is considered, which corresponds to nonlinear excitation of only one localized daughter upper-hybrid wave occurring as a result of the primary decay process. It is shown that, due to rather low instability threshold, it could hardly be completely suppressed in ECRH experiments using megawatt microwave beams. However, an increase in the radius of the pump wave cross section can considerably reduce the corresponding anomalous absorption.

Keywords: microwave heating, parametric decay instabilities, anomalous absorption of microwaves

DOI: 10.1134/S1063780X22040067

1. INTRODUCTION

Electron cyclotron resonance heating (ECRH) is widely used at current tokamaks and stellarators. It is planned to be used at future-generation toroidal facilities, such as the ITER [1] and DEMO [2] tokamak-reactors. This method is very promising due to the presence of reliable and relatively compact generators (gyrotrons) and the concept of local deposition of microwave power in the electron cyclotron (EC) resonance region [3], based, in particular, on the theoretical analysis that predicts the absence of nonlinear phenomena during the propagation of ordinary and extraordinary waves [4]. However, over the past two decades, a number of anomalous effects have been observed in experiments on ECR plasma heating, including the anomalous backscattering of microwaves [5–7], ion acceleration [8–10], and strong broadening of the power deposition profile [11–15]. These effects had no interpretation within the framework of the linear model of plasma-wave interaction. They had also no explanation within the framework of the nonlinear wave theory [4], which predicts extremely high thresholds for excitation of any nonlinear phenomena, including the parametric decay instabilities (PDIs), at least in the cases when the upper hybrid resonance (UHR) for the microwave is outside the plasma volume. To explain these anomalous phenomena, a new theoretical model was proposed that expands the concept of the nonlinear (parametric) phenomena development in inhomogeneous plasma, outlined in review [4], and takes into account the distinctive features of real density and magnetic field profiles, formed in toroidal facilities during the ECRH. With the help of the new model, it turned out to be possible to interpret all anomalous phenomena and effects as consequences of excitation of the low-threshold PDIs of pump waves. The key elements of the new theoretical model are as follows. First, it is the possibility of localizing the nonlinearly generated daughter waves (wave) along the direction of inhomogeneity, near the local maximums of the nonmonotonic density profiles, which are often observed in the ECRH experiments [16–18]. Second distinctive feature is the additional localization of the daughter waves at the magnetic surface due to the finite width of the pump beam. We note that the localization effect makes it possible to suppress the energy losses of daughter waves (wave) from the decay region and results in the possibility of excitation of an absolute PDI pump wave, as a result of which the amplitude of the daughter waves (wave) exponentially increases with time [19–25].

For typical conditions of experiments on the ECR plasma heating using microwaves of extraordinary polarization at the second harmonic of the EC resonance, the most dangerous scenario of the PDI pump wave formation is the two-plasmon decay resulting in the generation of two upper hybrid (UH) quasi-longi-

tudinal waves [21]. Most likely, the primary two-plasmon PDI becomes saturated due to two competing processes: the cascade of secondary decays [26–29] and depletion of the pump wave [30–32]. The analysis, the results of which can be found in [33–36], shows that regardless of the fact whether both primary daughter waves or only one of them are localized, the anomalous absorption is determined by the number of possible steps in the secondary decay cascade. If the number of steps in the cascade of secondary decays of the primary daughter wave(s) is odd, this cascade process will result in the instability saturation. However, in the case of an even number of secondary instabilities, the depletion of the pump wave plays a decisive role in the transition of the primary instability to the saturation regime, and it is responsible for the extremely high anomalous absorption (up to 80% of the pump power). It was shown in [27] that the main predictions of the developed theoretical model, in particular, the threshold power of the primary instability and the spectrum of secondary waves, are in reasonable agreement with the results obtained in the detailed study of anomalous backscattering at the TEXTOR tokamak [6]. We note that the possibility of strong anomalous absorption of the pump wave of extraordinary polarization in the ECRH experiments at the second harmonic of the EC resonance was experimentally discovered in the model experiments performed at the linear plasma facility [37].

Thus, the low-threshold two-plasmon decay can decrease the efficiency of auxiliary heating. This circumstance makes it important to find a way to avoid or reduce this parasitic effect. In a particular case, when both primary UH waves arising as a result of the parametric decay of the extraordinary pump wave can be localized in the vicinity of the density profile maximum, the method for reducing anomalous absorption was proposed in [38]. However, this case is very specific and can occur only in a narrow range of plasma parameters. In the general case, in the ECRH experiments, the extraordinary pump wave can decay into a trapped UH wave and not trapped UH (or extraordinary) wave. Just this decay scenario was observed at the ASDEX-Upgrade [39] and Wendelstein 7-X [40] facilities during their last experimental sessions. We note that, at both facilities, the PDI development was detected in a wide range of parameters during the passage of microwaves of extraordinary polarization through the plasma formation, in which the local density maximum was observed (rotating or stationary magnetic islands, the axis of the plasma column, ELMs (edge-localized modes)). Unfortunately, in this case, the instability saturation is described by completely different set of nonlinear equations as compared to [38]. For this reason, the results of the analysis presented in [38] and the approach to suppressing the anomalous effects proposed there are inapplicable in the general case.

To fill this theoretical gap, in this paper, we consider the possibility of reducing the anomalous absorption in the case for which the primary low-threshold decay results in the excitation of only one localized daughter UH wave, while the second daughter UH (or extraordinary) wave escapes from the region of nonlinear interactions along the direction of inhomogeneity. In this work, we analyze the cascades of secondary decays of the trapped primary UH wave with both odd and even number of steps. The effect of the pump wave depletion is also taken into account. As a result of the analysis performed, it is shown that an increase in the beam width of the pump wave can result in a decrease in the anomalous absorption of the extraordinary pump wave.

2. PRIMARY DECAY OF EXTRAORDINARY PUMP WAVE AND TWO MECHANISMS FOR ITS SATURATION

Parametric decay occurs in a small volume, in which the decay conditions are satisfied for the wave vectors and frequencies of the interacting waves. This makes it possible to use the Cartesian coordinate system (x, y, z), in which the x coordinate plays the role of a flux variable, which is directed inside the plasma column, while the y, z coordinates are directed across and along the magnetic field line on the magnetic surface. The origin of the coordinate system coincides with the local maximum of the upper hybrid (UH) frequency profile. We consider the monochromatic extraordinary (X) pump wave propagating quasi-perpendicularly to the external magnetic field. In the WKB approximation, it can be represented as follows:

$$\mathbf{E}_0 = \mathbf{e}_0 \frac{C_0(\mathbf{r})}{2}\sqrt{\frac{\omega_0}{k_x(\omega_0, x)c}} \times \exp\left(i\int^x k_x(\omega_0, x')dx' - i\omega_0 t\right) + \text{c.c.}, \quad (1)$$

where $\mathbf{e}_0 = \mathbf{e}_{0x} + \mathbf{e}_{0y} = \mathbf{e}_y - i\mathbf{e}_x\frac{g_0}{\varepsilon_0}$ is the polarization vector, $\mathbf{e}_{x,y}$ are the unit vectors along the corresponding direction, $k_x = \frac{\omega_0}{c}\sqrt{\varepsilon_0 - \frac{g_0^2}{\varepsilon_0}}$ is the local value of the wavenumber, and $g_0 = g(\omega_0)$ and $\varepsilon_0 = \varepsilon(\omega_0)$ are the perpendicular components of the cold plasma permittivity tensor [41]. In the WKB approximation, the potentials of the daughter UH waves (denoted by the "a" and "b" indices, where the first wave is localized in the vicinity of the maximum of the nonmonotonic

density profile, and the second is non-localized) can be represented in the following form [22, 23]:

$$\varphi_a = \frac{C_a}{2}\phi_m(x)\exp(-i\omega_m t) + \text{c.c.},$$
$$\varphi_b = \frac{C_b}{2}\exp\left(i\int_0^x q_x^-(\omega_0-\omega_m,x')dx' + i(\omega_0-\omega_m)t\right) + \text{c.c.}, \quad (2)$$

where the eigenfunction [21]

$$\phi_m(x) = \frac{1}{\sqrt{L_m^+(x)}}\exp\left(i\int_{x_l^*}^x q_x^+(\omega_m,\xi)\,d\xi - i\frac{\pi}{4}\right) + \frac{1}{\sqrt{L_m^-(x)}}\exp\left(i\int_{x_l^*}^x q_x^-(\omega_m,\xi)\,d\xi + i\frac{\pi}{4}\right), \quad (3)$$
$$L_m^\pm(x) = \left|D_q^\pm(x)\right|\int_{x_l^*}^{x_r^*} d\xi\left(\left|D_q^+(\xi)\right|^{-1} + \left|D_q^-(\xi)\right|^{-1}\right)$$

describes the localization of the "a" wave along the x coordinate. In expressions (2) and (3), the wave numbers $q_x^\pm(\omega,\xi)$ correspond to the "warm" (+) and "cold" (−) solutions to the local dispersion equation for the UH wave $D_{UH}\left(\omega_m, q_x^\pm\right) = 0$, obtained for $q_y = 0$ and $q_z = 0$, and $D_q^\pm = \partial D_{UH}/\partial q_x\big|_{q_x^\pm(\omega,x)}$. The explicit form of the dispersion equation can be found in [21, 41]. The frequency of the localized wave obeys the Bohr–Sommerfeld quantization condition [21] $\int_{x_l^*}^{x_r^*} q_x^+(\omega_m,\xi)\,d\xi + \int_{x_r^*}^{x_l^*} q_x^-(\omega_m,\xi)\,d\xi = \pi(2m+1)$, where $x_{l,r}^*$ are two solutions to the equation $D_q(x_{l,r}^*) = 0$. In the absence of nonlinear coupling, the $C_{0,a,b}$ amplitudes of all waves in expressions (1) and (2) are constant. After the instability excitation, they cease to be constant. In particular, under the natural assumption of weak diffraction of pump wave (1), its depletion as a result of decay is described by the following equation, which was obtained for the first time in [35]:

$$\frac{\partial C_0}{\partial x} = -i\frac{\omega_0}{2cB_0}\chi_e^{(p)}C_a\phi_m C_b^* \times\exp\left(-i\int^x\left(q_x^-(x') + k_0(x')\right)dx'\right). \quad (4)$$

The boundary condition for the $C_0(\mathbf{r})$ amplitude of the pump wave falling onto the plasma layer, in which the nonlinear interaction occurs, has the following form:

$$C_0\big|_{-\infty} = \sqrt{\frac{8P_0}{cw^2}}\exp\left(-\frac{y^2}{2w^2} - \frac{z^2}{2w^2}\right), \quad (5)$$

where P_0 and w are the beam power and width. In expression (4), B_0 is the magnetic field induction in the decay region, and $\chi_e^{(p)}$ is the plasma nonlinear susceptibility, which describes the interaction of two longitudinal waves and the extraordinary wave [42].

The amplitude of the second traveling UH wave φ_b, escaping from the interaction region and propagating towards the plasma boundary is described by the following equation:

$$\frac{\partial C_b}{\partial x} = -iC_aC_0^*\frac{\chi_e^{(p)}}{2B_0}\frac{\phi_m}{D_q^-(\omega_0-\omega_m,x)} \times\exp\left(-i\int^x\left(q_x(x') + k_0(x')\right)dx'\right) \quad (6)$$

with the boundary condition $C_b\big|_\infty = 0$. We integrate Eq. (6) and substitute the resulting amplitude into Eq. (4) and into the equation that describes the localized UH wave. As a result, after integrating the equation for the trapped UH wave over the x coordinate with the $\phi_m(x)^*$ weight, we obtain the following set of integro-differential equations [35, 36] for the pump wave and the trapped UH wave:

$$\begin{cases}\dfrac{\partial}{\partial\xi}a_0 = -\gamma_p\dfrac{T_e}{P_0}\dfrac{\omega_0}{\omega_m}|a_m(y,z)|^2 \\ \times\displaystyle\int_\xi^\infty d\xi'\,a_0(\xi')\exp\left(i\Psi_p(\xi) - i\Psi_p(\xi')\right) \\ \dfrac{\partial a_m}{\partial t} - i\Lambda_{my}\dfrac{\partial^2 a_m}{\partial y^2} - i\Lambda_{mz}\dfrac{\partial^2 a_m}{\partial z^2} \\ = \tilde\gamma_p a_m W(t,y,z;a_0)\exp\left(-\dfrac{y^2}{w^2} - \dfrac{z^2}{w^2}\right).\end{cases} \quad (7)$$

In Eqs. (7), a_0 and a_m are the dimensionless amplitudes of the pump wave and the trapped UH wave, respectively, defined as follows: $C_0 = \sqrt{8P_0/\left(\upsilon_{0g}w^2\right)}a_0$ and $C_a = \sqrt{16T_e/(\omega_m\langle D_{m\omega}\rangle w^2)}\,a_m$, where υ_{0g} is the projection of the group velocity of the pump wave onto the direction of plasma inhomogeneity. In Eqs. (7), $\Psi_p(\xi) = \xi^3 - \lambda_p\xi$ is the phase arising as a result of mismatch of the decay condition for the wave numbers of interacting waves in inhomogeneous plasma during the development of the primary instability $\Delta K_p = k_x(\omega_0,x) + q_x^-(\omega_0-\omega_m,x) - q_x^-(\omega_m,x)$; $\xi = x/l_{dp}$, and $\lambda_p = \Delta K_p(x_{dp})l_{dp}$, where x_{dp} is the coordinate of the point, in which the ΔK_p function has an extremum and $l_{dp} = \left|d^2\Delta K_p/dx^2\right|_{x_{dp}}^{-1/3}/6^{-1/3}$; $\Lambda_{my,z} = \langle\partial^2 D_{UH}/(2\partial q_{y,z}^2)\rangle\langle D_{m\omega}\rangle^{-1}$ are the diffraction

coefficients averaged over the region of the UH wave localization; $\langle D_{m\omega}\rangle = \langle|\partial D_{UH}/\partial\omega|_{\omega_m}\rangle$; the averaging procedure is described as $\langle ...\rangle = \int_{x_l^*}^{x_r^*} dx...|\phi_m(x)|^2$, and

$$W(t,y,z;a_0) = \int_{-\infty}^{\infty}\int_{\xi}^{\infty}\frac{d\xi d\xi'}{F(\lambda_p)}a_0(\xi)a_0^*(\xi')$$

$$\times\exp\left(i\lambda_p(\xi-\xi') - i\left(\xi^3-\xi'^3\right)\right), \quad (8)$$

$$F(\lambda_p) = \int_{-\infty}^{\infty} d\xi\int_{\xi}^{\infty} d\xi'\exp\left(i\lambda_p(\xi-\xi') - i\left(\xi^3-\xi'^3\right)\right).$$

In the case of weak depletion of the pump wave, i.e. when the dimensionless amplitude of the pump wave is close to unity $a_0 \le 1$, representation (8) can be reduced to $W(t) = 1$. Otherwise, function (8) obeys the inequality $W(t) < 1$. In addition, in set of Eqs. (7), we used the coefficient that describes the nonlinear pumping of the daughter UH wave $\tilde{\gamma}_p = \gamma_p F(\lambda_p)$, where

$$\gamma_p = \frac{\left|\chi_e^{(p)}\right|^2 l_{dp}^2}{\left|L_m^-\right|\left|D_q^-(\omega_0-\omega_m)\right|\langle D_{m\omega}\rangle}\frac{2P_0}{\upsilon_{0g}w^2B_0^2}\Bigg|_{x_{dp}} \propto \frac{P_0}{w^2}. \quad (9)$$

As can be seen from expression (9), the γ_p coefficient depends on the pumping power and is inversely proportional to the square of the beam width.

Thus, the set of Eqs. (7) describes the instability of the extraordinary pump wave with allowance for its depletion. In set of Eqs. (7), it is the depletion effect that results in the instability saturation. Meanwhile, this is not the only mechanism for the instability transition to the saturation regime. Subsequent decays of the primary localized UH wave can also result in the instability saturation. Let us consider the secondary instability of the localized primary UH wave, which leads to the excitation of the trapped UH wave and the ion Bernstein (IB) wave escaping from the decay region along the direction of plasma inhomogeneity. The first assumption makes it possible to minimize the losses of secondary UH waves from the decay region and increase the efficiency of the three-wave interaction [36]. Accounting for the secondary instability modifies Eqs. (7) in the following way [35, 36]:

$$\begin{cases}\dfrac{\partial}{\partial\xi}a_0 = -\gamma_p\dfrac{T_e}{P_0}\dfrac{\omega_0}{\omega_m}|a_m(y,z)|^2\displaystyle\int_{\xi}^{\infty}d\xi' a_0(\xi')\exp\left(i\Psi_p(\xi) - i\Psi_p(\xi')\right)\\ \dfrac{\partial a_m}{\partial t} - i\Lambda_{my}\dfrac{\partial^2 a_m}{\partial y^2} - i\Lambda_{mz}\dfrac{\partial^2 a_m}{\partial z^2} = \tilde{\gamma}_p a_m W(t,y,z)\exp\left(-\dfrac{y^2}{w^2}-\dfrac{z^2}{w^2}\right) - \sqrt{\dfrac{\omega_m}{\omega_n}}\tilde{\gamma}_s|a_n|^2 a_m\\ \dfrac{\partial a_n}{\partial t} + i\Lambda_{ny}\dfrac{\partial^2 a_n}{\partial y^2} + i\Lambda_{nz}\dfrac{\partial^2 a_n}{\partial z^2} = \sqrt{\dfrac{\omega_n}{\omega_m}}\tilde{\gamma}_s|a_m|^2 a_n,\end{cases} \quad (10)$$

where $\tilde{\gamma}_s = \gamma_s F(\lambda_s)^*$, the F function is defined above in Eq. (8), the coefficient

$$\gamma_s = \frac{4|e|^2}{\sqrt{\omega_m\omega_n}T_e}\frac{\left|\chi_e^{(s)}\right|^2}{\left|L_m^+\right|\left|L_n^+\right|\langle D_{m\omega}\rangle\langle D_{n\omega}\rangle|D_{Iq}|w^2}\frac{l_{ds}^2}{w^2}\Bigg|_{x_{ds}} \propto \frac{1}{w^2} \quad (11)$$

describes the secondary instability (it is inversely proportional to the square of the beam width), $\lambda_s = \Delta K_s(x_{ds})l_{ds}$, x_{ds} is the coordinate of the point, in which the ΔK_s detuning of the decay condition for the secondary instability has an extremum, and $l_{ds} = \left|d^2\Delta K_s/dx^2\right|_{x_{ds}}^{-1/3}/6^{-1/3}$. In set of Eqs. (10), we also introduced the dimensionless amplitude a_n of the secondary UH wave, which is defined in the same way as the a_m amplitude. In expression (11), $\chi_e^{(s)}$ is the nonlinear plasma susceptibility, which describes the nonlinear coupling of three longitudinal waves [42]; $D_{Iq} = |\partial D_{IB}/\partial q_x|_{q_{Ix}}$, q_{Ix} is the solution to the dispersion equation $D_{IB} = 0$ for the ion Bernstein wave [41]. A detailed derivation of Eqs. (7) and (10) can be found in [35, 36].

Depending on the depth of the "potential well," in which the primary UH wave can be localized, a different number of successive secondary decays is possible. The sequence of secondary decays ends with a decay leading to the excitation of a non-localized UH wave, since this process does not result in the absolute instability development, but only in the spatial amplification of the UH wave. The corresponding spatial gain factor can be estimated as follows [36]:

$$\Gamma_d = \exp\left(\frac{2\pi l_d^2\tilde{\gamma}_d^2}{|\upsilon_{IBg}||\upsilon_{UHg}|}\right) \simeq \exp\left(\alpha\frac{q_{Ix}^4 l_d^2|\phi_p|^2}{B_0^2}\right),$$

where α is the dimensionless coefficient depending on plasma parameters; $\tilde{\gamma}_d = \tilde{\gamma}_d(|\phi_p|)$ is the instability growth rate determined in homogeneous plasma, which depends on the amplitude of the decaying localized UH-wave; l_d is the size of the resonance layer; υ_{UHg} and υ_{IBg} are the group velocities of the daughter UH and IB waves at the x_d decay point; and q_{Ix} is the solution to the dispersion equation $D_{IB} = 0$ for the daughter ion Bernstein wave [41]. For typical experimental conditions, the gain factor obeys the inequality $\ln(\Gamma_d) < 1$ indicating the absence of spatial amplification, which interrupts the cascade of successive decays.

We note that each of the IB waves participating in the decay cascades has its own unique frequency, at which the optimal coupling with the eigenmodes of the UH waves is ensured. In this case, the discrepancy of the resonance condition for the wave vectors of interacting oscillations can be described by a parabola, which is typical for the case of two close decay points. In the following sections, we analyze two cases corresponding to the odd and even number of secondary instabilities. We will start from analyzing the first of them.

3. SUPRESSION OF ANOMALOUS ABSORPTION IN THE CASE OF ODD NUMBER OF SECONDARY DECAYS

We consider the case of small amplitude of the local density maximum, which was characteristic of the ECRH experiments that were carried out at the TEXTOR tokamak [5, 6]. The frequency profile of the UH wave is shown in Fig. 1 by solid line. The scale characterizing the depth and size of the potential well is $l_w = (d^2 \ln f_{UH}/(2dx^2))^{-1/2} = 11.31$ cm. The wavenumbers of the primary and secondary UH waves are shown by solid and dash-and-dot curves. The frequency of the primary wave is $f_m = 70.6$ GHz ($m = 0$). The frequency of the secondary wave is $f_n = 70.582$ GHz ($n = 1$). The pump wave frequency is $f_0 = 140$ GHz. Parameters in the local maximum of the UH-frequency profile are as follows: $T_e = 600$ eV and $f_{ce} = 51.72$ GHz. The cascade of decays resulting in the excitation of UH waves, the dispersion curves of which are shown in Fig. 1, is described by set of Eqs. (10). We begin analyzing these equations with an analytical consideration. As was shown in [35, 36], in this case, the dominant mechanism responsible for the transition of the instability to the saturated regime is the secondary instability, which makes it possible to

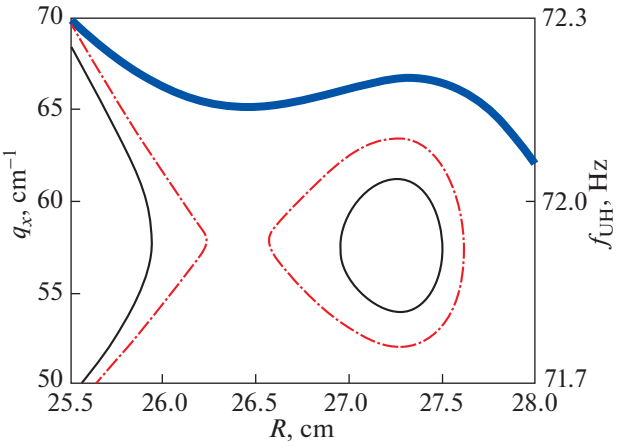

Fig. 1. Dispersion curves of localized UH waves (solid and dash-and-dot lines correspond to $f_m = 70.6$ GHz and $f_n = 70.582$ GHz, respectively). UH frequency profile is shown by thick solid line. $T_e = 600$ eV and $f_{ce} = 51.72$ GHz in the local maximum of density profile. $l_w = (d^2 \ln f_{UH}/(2dx^2))^{-1/2} = 11.31$ cm.

neglect the pump wave depletion effect and reduce set of Eqs. (10) to the following set of equations:

$$\begin{cases} \dfrac{\partial a_m}{\partial t} - i\Lambda_{my}\dfrac{\partial^2 a_m}{\partial y^2} - i\Lambda_{mz}\dfrac{\partial^2 a_m}{\partial z^2} \\ = \tilde{\gamma}_p a_m \exp\left(-\dfrac{y^2}{w^2} - \dfrac{z^2}{w^2}\right) - \sqrt{\dfrac{\omega_m}{\omega_n}}\tilde{\gamma}_s |a_n|^2 a_m \\ \dfrac{\partial a_n}{\partial t} + i\Lambda_{ny}\dfrac{\partial^2 a_n}{\partial y^2} + i\Lambda_{nz}\dfrac{\partial^2 a_n}{\partial z^2} = \sqrt{\dfrac{\omega_n}{\omega_m}}\tilde{\gamma}_s |a_m|^2 a_n. \end{cases} \quad (12)$$

The primary instability described by the first equation in set of Eqs. (12) begins to develop if the pump wave power exceeds the P_0^{th} threshold power. If the pump wave power considerably exceeds the threshold power, $P_0 \gg P_0^{th}$, then the instability growth rate can be obtained analytically [35, 36]

$$\nu_{k,l} = \tilde{\gamma}_p' - \left((2k+1)\sqrt{\frac{\tilde{\gamma}_p|\Lambda_{my}|}{w^2}} + (2l+1)\sqrt{\frac{\tilde{\gamma}_p|\Lambda_{mz}|}{w^2}}\right) \times \sin\left(\frac{\arctan(F''/F')}{2} + \frac{\pi}{4}\right) \propto \frac{1}{w^2}, \quad k,l \in \mathbb{Z}, \quad (13)$$

where $\tilde{\gamma}_p \equiv \tilde{\gamma}_p' + i\tilde{\gamma}_p'' = \gamma_p(0,0)F(\lambda_p)$ and $\gamma_p(0,0) \sim P_0/w^2$ (see Eq. (9)). Although expression (13) becomes incorrect when the beam power is of the order of the threshold power $P_0 \approx P_0^{th}$, we can use it to roughly estimate the instability threshold. To

this purpose, we substitute $\nu_{k,l} = 0$ in expression (13) and obtain the following equation for the threshold:

$$\tilde{\gamma}_{\rm p}'\left(P_0^{th}\right) = \frac{\left|\tilde{\gamma}_{\rm p}'\left(P_0^{th}\right)\right|^{1/2}}{w}\left((2k+1)\sqrt{\Lambda_{my}} + (2l+1)\sqrt{\Lambda_{mz}}\right) \times \sin\left(\frac{\arctan\left(F''/F'\right)}{2} + \frac{\pi}{4}\right). \quad (14)$$

Since $|\tilde{\gamma}_{\rm p}'| \sim P_0^{th}/w^2$, the left and right sides of Eq. (14) are proportional to $1/w^2$. This allows us concluding that the instability threshold power does not depend on the beam width, i.e., $P_0^{th} \propto w^0$. In the specific case of nonlinear excitation of two localized UH waves, shown in Fig. 1, the threshold power is $P_0^{th} \approx 107$ kW. Next, we analyze how the saturation level of all daughter waves depends on the width of the pump beam. The regime of the instability saturation described by Eqs. (12) corresponds to its stationary solutions. The levels of the energy density saturation of the parametrically excited UH waves can be estimated by analyzing the balance of sources and sinks in these equations. The level of energy density saturation $\varepsilon_m^{\rm s} = |a_m^{\rm s}|^2$ of the primary UH waves in the pump beam is determined by the balance between the secondary decay rate $\nu_{\rm s}\varepsilon_m^{\rm s}$ and diffraction energy losses of secondary waves from the pump beam cross section:

$$\varepsilon_m^{\rm s} \approx \frac{1}{\tau_n|\tilde{\gamma}_{\rm s}|} \propto w^0 P_0^0, \quad (15)$$

where $\tau_n = \min\left(w^2/\Lambda_{\rm v}, w^2/\Lambda_{nz}\right) \approx w^2/\Lambda_{nz}$. The energy density $\varepsilon_n^{\rm s} = |a_n^{\rm s}|^2$ of the secondary UH waves in the pump beam cross section is determined by the balance between the primary instability growth rate and energy losses due to the secondary decay

$$\varepsilon_n^{\rm s} \approx \frac{|\tilde{\gamma}_{\rm p}|}{|\tilde{\gamma}_{\rm s}|} \propto P_0. \quad (16)$$

As can be seen, the saturation levels of both the primary and secondary daughter waves remain independent of the pump beam width, but the saturation level of the secondary UH wave linearly depends on the pump wave power. Nevertheless, a change in the beam width can affect the efficiency of energy loss of the daughter waves from the pump beam cross section and the efficiency of nonlinear energy transport from the pump wave to these daughter waves.

In the case of weak depletion of the pump wave, we can describe this phenomenon using the perturbation theory procedure, assuming $a_0 \simeq 1 - \delta a_0$, where $|a_0| \gg |\delta a_0|$ [35]. In this approximation, a change in the pump wave energy flux along the x coordinate can be estimated as follows:

$$\delta S_x \approx \frac{2P_0}{\pi w^2}|\delta a_0|\exp\left(-\frac{y^2}{2w^2} - \frac{z^2}{2w^2}\right), \quad (17)$$

where the correction term δa_0 to the pump wave amplitude obeys the first equation of set of Eqs. (7). Integrating Eq. (17) over the x coordinate, after simple calculations, we obtain the expression that, in the limit $x \to \infty$, is as follows:

$$\delta a_0 \approx \frac{\tilde{\gamma}_{\rm p} T_e}{P_0}\frac{\omega_0}{\omega_m}|a_m(y,z)|^2. \quad (18)$$

Substituting expression (18) into Eq. (17), we obtain

$$\delta S_x = \tilde{\gamma}_{\rm p}\frac{2T_e}{\pi w^2}\frac{\omega_0}{\omega_m}|a_m(y,z)|^2\exp\left(-\frac{y^2}{2w^2} - \frac{z^2}{2w^2}\right). \quad (19)$$

Next, we integrate both parts of Eq. (19) over the y and z variables. Estimating the double integral as

$$\int_{-\infty}^{\infty} dydz\,|a_m(y,z)|^2\exp\left(-\frac{y^2}{2w^2} - \frac{z^2}{2w^2}\right) \approx 2\pi w^2\varepsilon_m^{\rm s}$$

and bearing in mind that $\Delta P = \delta S_x \pi w^2$, we finally obtain:

$$\frac{\Delta P}{P_0} \approx \tilde{\gamma}_{\rm p}\frac{8T_e}{P_0}\varepsilon_m^{\rm s} \propto \frac{1}{w^2}. \quad (20)$$

Thus, the fraction of the pump power received by the daughter waves inversely depends on the cross-sectional area of the beam and remains independent of the pump power.

To verify this prediction, assuming the initial heat level of all UH waves, we numerically solve Eqs. (10) with allowance for the pump wave depletion. The results of the numerical solution are shown in Fig. 2 for the beam radius and pumping power of $w = 1$ cm and $P_0 = 600$ kW, respectively. The figure shows the dimensionless energy densities of the primary and secondary UH waves averaged over the pump beam in accordance with the following mathematical procedure:

$$\langle\varepsilon_{m,n}\rangle = \int_S \frac{dydz}{\pi w^2}|a_{m,n}(y,z)|^2\exp\left(-\frac{y^2}{w^2} - \frac{z^2}{w^2}\right)$$

and plotted on a semi-logarithmic scale. Solid and dashed curves correspond to the energies of primary and secondary UH waves, respectively. Thin horizontal lines are the estimates of saturation levels (15) and (16). They are in reasonable agreement with the numerical results. The primary instability is well described by the analytical formula (13) used for the fundamental modes in the directions of both y and z coordinates (see dashed line). The agreement between the theoretical estimates and the results of the numerical solution of the set of nonlinear partial differential equations makes it possible to feel confidence in the

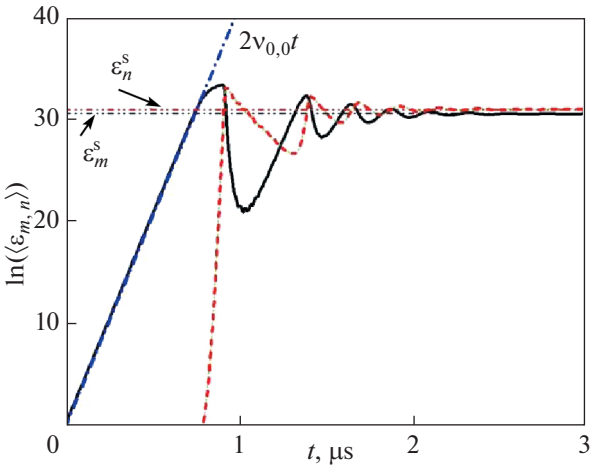

Fig. 2. Time dependences of energies of primary (solid line) and secondary (dashed line) plasmons in the beam cross section are shown on semi-logarithmic scale. An increase in primary UH wave amplitude is adequately described (dash-and-dot line) by growth rate (13). Thin horizontal lines are saturation levels (15) and (16). Parameters are the same as in Fig. 1, $w = 1$ cm, and $P_0 = 600$ kW.

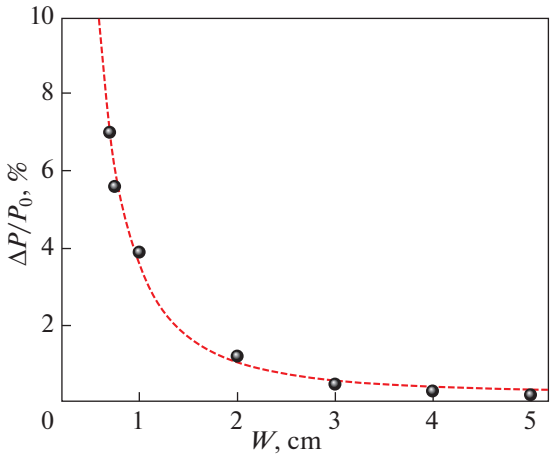

Fig. 3. Anomalous absorption coefficient as a function of the w pump beam radius. Symbols correspond to results of numerical solution. Dashed line shows analytical prediction (20). $P_0 = 1$ MW.

performed calculations. The anomalous absorption coefficient as a function of the w pump beam radius is shown in Fig. 3. The symbols show the result of a numerical solution. The dotted line corresponds to the analytical prediction (20). The heating power is $P_0 =$ 1 MW. We see that in the case of weak anomalous absorption, the analytical dependence is in reasonable agreement with the results of the numerical solution. This case is characteristic of odd number of secondary decays resulting in the instability saturation. The fraction of the anomalously absorbed pump power decreases with increasing beam radius. The anomalous absorption coefficient as a function of the pumping power is shown in Fig. 4. The dependences are shown obtained both as a result of numerical simulation and in accordance with the analytical estimate (20). As predicted by the analytical estimate (20), the growth rate of this dependence saturates at $P_0 \gg P_0^{th}$ (see dashed line).

4. ANOMALOUS ABSORPTION IN THE CASE OF EVEN NUMBER OF SECONDARY DECAYS

Next, we consider the nonmonotonic density profile with a larger difference between the maximum and minimum densities than in the previous section, which makes possible the occurrence of an even number of successive secondary decays of the primary UH wave. This case is illustrated in Fig. 5, which shows the dispersion curves of all eigenmodes excited as a result of the cascade process during the development of decay instability of the pump wave. The solid line corresponds to the fundamental mode $m = 0$, $f_m = 70.74$ GHz. The dashed-dotted line corresponds to $n = 1$, $f_n = 70.72$ GHz. The dashed line corresponds to $r = 2$, $\omega_r/2\pi = 70.7$ GHz. The UH frequency profile is shown by the thick solid line. The scale characterizing the depth and size of the potential well is $l_w = (d^2 \ln f_{UH}/(2dx^2))^{-1/2} = 13.2$ cm. The dispersion curves are shown for the following plasma parameters: $T_e = 600$ eV and $f_{ce} = 51.72$ GHz. The decay of the $r = 2$ mode could lead to the appearance of nonlocalized UH and IB waves. However, the threshold power for this phenomenon is higher than the power of the $r = 2$ UH-wave mode, as a result of which the cascade of successive decays is terminated. According to [35, 36], this cascade excitation of three

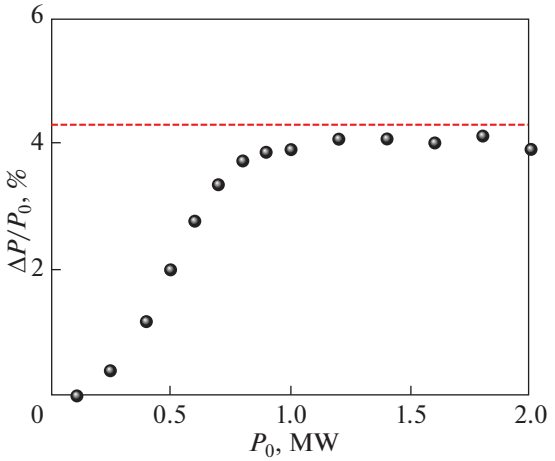

Fig. 4. Anomalous absorption coefficient as a function of pump beam power. Symbols correspond to results of numerical solution. Dashed line shows analytical prediction (20). $w = 1$ cm.

eigenmodes of the UH wave can be described by the following set of equations:

$$\begin{cases} \dfrac{\partial}{\partial\xi}a_0 = -\gamma_p\dfrac{T_e}{P_0}\dfrac{\omega_0}{\omega_m}|a_m(y,z)|^2 \\ \times\displaystyle\int_\xi^\infty d\xi' a_0(\xi')\exp\left(i\Psi_p(\xi)-i\Psi_p(\xi')\right) \\ \dfrac{\partial a_m}{\partial t}-i\Lambda_{my}\dfrac{\partial^2 a_m}{\partial y^2}-i\Lambda_{mz}\dfrac{\partial^2 a_m}{\partial z^2}=\tilde\gamma_p a_m W(t,y,z;a_0) \\ \times\exp\left(-\dfrac{y^2}{w^2}-\dfrac{z^2}{w^2}\right)-\sqrt{\dfrac{\omega_m}{\omega_n}}\tilde\gamma_s|a_n|^2 a_m \\ \dfrac{\partial a_n}{\partial t}+i\Lambda_{ny}\dfrac{\partial^2 a_n}{\partial y^2}+i\Lambda_{nz}\dfrac{\partial^2 a_n}{\partial z^2} \\ =\sqrt{\dfrac{\omega_n}{\omega_m}}\tilde\gamma_s|a_m|^2 a_n-\sqrt{\dfrac{\omega_n}{\omega_r}}\tilde\gamma_t|a_r|^2 a_n \\ \dfrac{\partial a_r}{\partial t}-i\Lambda_{ry}\dfrac{\partial^2 a_r}{\partial y^2}-i\Lambda_{rz}\dfrac{\partial^2 a_r}{\partial z^2}=\sqrt{\dfrac{\omega_r}{\omega_n}}\tilde\gamma_t|a_n|^2 a_r, \end{cases} \quad (21)$$

where $\tilde\gamma_t=\gamma_t F(\lambda_t)$, γ_t describes the tertiary instability, $\lambda_t=\Delta K_t(x_{dt})l_{dt}$, x_{dt} is the coordinate of the point, at which the ΔK_t mismatch has a local minimum during the tertiary instability development, and $l_{dt}=\left(\partial^2\Delta K_t/(6\partial x^2)\right)^{-1/3}$. The depletion of the pump wave $a_0\left(\xi,\varepsilon_m^s\right)$, which in this case, is the dominant mechanism for the instability saturation and is responsible for the considerable anomalous absorption of the pump wave, is described by the first of Eqs. (21). To estimate the levels of decay waves in the regime of PDI saturation, we discard all terms containing time derivatives and replace the derivatives with their rough estimates $\partial/\partial y,\partial/\partial z\to 1/w$. The level of saturation of the energy density $\varepsilon_n^s=|a_n^s|^2$ of secondary UH waves in the pump beam is determined by the balance between the growth rate of tertiary waves and the energy loss of tertiary waves from the pump beam cross section characterized by time $1/\tau_r=\max\left(\Lambda_{ry},\Lambda_{rz}\right)/w^2$, i.e.,

$$\varepsilon_n^s\approx\sqrt{\frac{\omega_n}{\omega_r}}\frac{1}{\tilde\gamma_t\tau_r}\propto w^0. \quad (22)$$

The energy density of the primary UH wave $\varepsilon_m^s=|a_m^s|^2$ becomes saturated in the pump beam cross section due to the pump wave depletion and its secondary decay. The level of depletion sufficient to terminate the primary instability development can be estimated by numerically evaluating the following balance equation:

$$W=\sqrt{\frac{\omega_m}{\omega_n}}\frac{\tilde\gamma_s}{\tilde\gamma_p}\varepsilon_n^s. \quad (23)$$

Since the W function depends on the a_0 amplitude (see Eq. (8)), and the a_0 amplitude is a function of ε_m^s, the left side of Eq. (23) depends on ε_m^s, i.e., $W=W\left(\varepsilon_m^s\right)$. In the stationary regime, the first terms on the right-hand sides of the third and fourth equations in set of Eqs. (21) balance the second ones, which makes it possible to find the levels of saturation of the energy density of the secondary UH waves $\varepsilon_r^s=|a_r^s|^2$ in the pump beam:

$$\varepsilon_r^s\approx\sqrt{\frac{\omega_r}{\omega_m}}\frac{\tilde\gamma_s}{\tilde\gamma_t}\varepsilon_m^s. \quad (24)$$

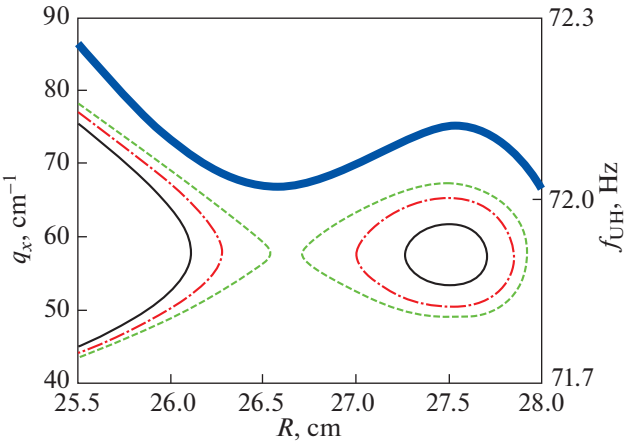

Fig. 5. Dispersion curves of nonlinearly coupleD UH waves (solid line corresponds to $m=0$ and $f_m=70.74$ GHz; dash-and-dot line corresponds to $n=1$ and $f_n=70.72$ GHz; and dashed line corresponds to $r=2$ and $f_r=70.7$ GHz). UH frequency profile is shown by thick solid line. $T_e=600$ eV, $f_{ce}=51.72$ GHz, and $l_w=(d^2\ln f_{UH}/(2dx^2))^{-1/2}=13.2$ cm.

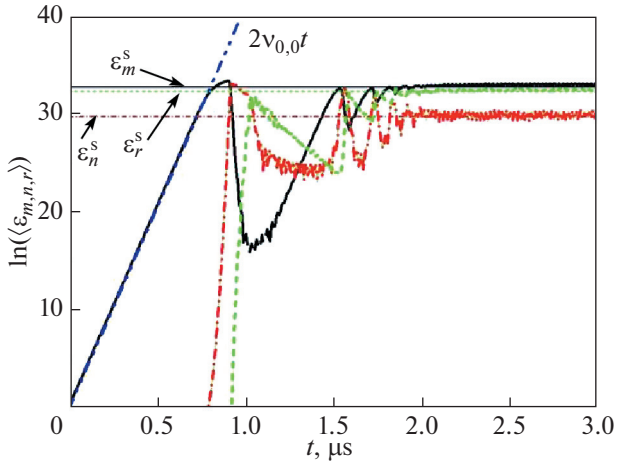

Fig. 6. Time dependences of energies of primary (solid line), secondary (dash-and-dot line), and tertiary (dashed line) plasmons in the beam cross section are shown on semi-logarithmic scale; the dash-and-dot line $2\nu_{0,0}t$ is determined by Eq. (13). Thin horizontal lines are saturation levels (10) and (11). Parameters are the same as in Fig. 5, $w=1$ cm and $P_0=1$ MW.

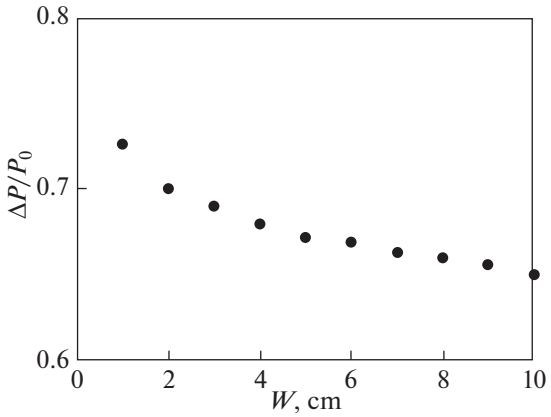

Fig. 7. Anomalous absorption coefficient as a function of pump beam radius. Pumping power is $P_0 = 1$ MW.

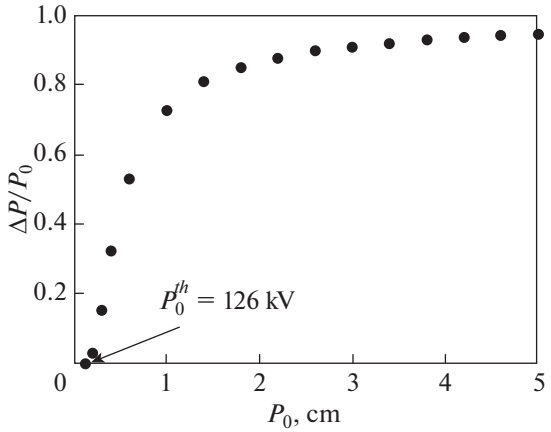

Fig. 8. Anomalous absorption coefficient as a function of pumping power. Beam radius is $w = 1$ cm.

Unfortunately, it is not possible to find ε_m^s analytically. This estimate can be obtained only numerically as a result of solving Eq. (23).

Next, we numerically find the solution to set of Eqs. (21). The results of solving Eqs. (21) under the conditions used previously when calculating the dispersion curves shown in Fig. 5 ($w = 1$ cm, $P_0 = 1$ MW), are presented in Fig. 6, which shows the dimensionless energies averaged over the pump beam cross section of the corresponding daughter waves excited during the cascade decays. The exponential growth of the primary UH wave (solid line) is adequately described by the gain factor (dash-dotted line) calculated using the growth rate (13). The energies of the secondary and tertiary waves are shown by dash-and-dot and dashed curves, respectively. Estimates (22)–(24) of the levels of amplitude saturation of the daughter waves found as a result of numerically solving Eq. (23), are shown in the figure by thin horizontal lines. It can be seen that they are in reasonable agreement with the results of numerically solving set of Eqs. (21). The anomalous absorption coefficient as a function of the pump beam radius is shown in Fig. 7 for the pumping power $P_0 = 1$ MW. The dependence demonstrates that the anomalous absorption decreases only slightly with increasing beam width. The anomalous absorption coefficient as a function of the pumping power is shown in Fig. 8 for $w = 1$ cm. The anomalous absorption coefficient increases with power, asymptotically approaching unity ($\Delta P/P_0 \to 1$) at a power level of several megawatts, which corresponds to the total anomalous absorption.

5. CONCLUSIONS

Summarizing the results of the study, we can conclude that the anomalous absorption of microwaves caused by the development of their low-threshold PDI, during which only one localized UH wave is excited, can be reduced by increasing the pump beam radius. This conclusion is similar to that made in the case when the primary parametric decay results in the excitation of two localized UH waves [38]. An increase in the pump beam radius is useful in the case of odd number of secondary decays of the primary UH wave, when the anomalous absorption can be considerably reduced. In the case of development of an even number of successive secondary instabilities, the effect of the pump beam width on the level of anomalous absorption is weaker. In this case, an increase in the pumping power results in an increase in the rate of anomalous absorption, which distinguishes the case considered in this study from the case, in which two localized UH waves are excited during the first parametric decay [38].

FUNDING

The analytical treatment presented in Sections 1–3 was supported by the Ioffe Institute under the State Contract No. 0040-2019-0023, while the numerical simulations described in Sections 3 and 4 were supported by the Ioffe Institute under the State Contract No. 0034-2021-0003.

CONFLICT OF INTEREST

The authors declare that they have no conflicts of interest.

REFERENCES

1. O. Sauter, M. A. Henderson, G. Ramponi, H. Zohm, and C. Zucca, Plasma Phys. Control. Fusion **52**, 025002 (2010).
2. T. Franke, G. Aiello, K. Avramidis, C. Bachmann, B. Baiocchi, C. Baylard, A. Bruschi, D. Chauvin, A. Cufar, R. Chavan, C. Gliss, F. Fanale, L. Figini, G. Gantenbein, S. Garavaglia, et al., Fusion Eng. Des. **168**, 112653 (2021).
3. A. G. Litvak, G. G. Denisov, and M. Glyavin, IEEE J. Microwaves **1**, 260 (2021).
4. B. I. Cohen, R. H. Cohen, W. M. Nevins, and T. D. Rognlien, Rev. Mod. Phys. **63**, 949 (1991).
5. E. Westerhof, S. K. Nielsen, J. W. Oosterbeek, M. Salewski, M. R. de Baar, W. A. Bongers, A. Bürger, B. A. Hennen, S. B. Korsholm, F. Leipold, D. Moseev, M. Stejner, and D. J. Thoen, Phys. Rev. Lett. **103**, 125001 (2009).
6. S. K. Nielsen, M. Salewski, E. Westerhof, W. Bongers, S. B. Korsholm, F. Leipold, J. W. Oosterbeek, D. Moseev, and M. Stejner, Plasma Phys. Control. Fusion **55**, 115003 (2013).
7. G. M. Batanov, V. D. Borzosekov, L. M. Kovrizhnykh, L. V. Kolik, E. M. Konchekov, D. V. Malakhov, A. E. Petrov, K. A. Sarksyan, N. N. Skvortsova, V. D. Stepakhin, and N. K. Kharchev, Plasma Phys. Rep. **39**, 444 (2013).
8. S. Coda and the TCV Team, Nucl. Fusion **55**, 104004 (2015).
9. B. Zurro, A. Baciero, V. Tribaldos, M. Liniers, Á. Cappa, A. Lopez-Fraguas, D. Jiménez-Rey, J. M. Fontdecaba, O. Nekhaieva, and the TJ-II Team, Nucl. Fusion **53**, 083017 (2013).
10. M. Martínez, B. Zurro, A. Baciero, D. Jiménez-Rey, and V. Tribaldos, Plasma Phys. Control. Fusion **60**, 025024 (2018).
11. D. G. Vasilkov, G. M. Batanov, M. S. Berezhetskii, V. D. Borzosekov, S. E. Grebenshchikov, N. K. Kharchev, Yu. V. Khol'nov, L. V. Kolik, E. M. Konchekov, A. A. Letunov, V. P. Logvinenko, D. V. Malakhov, A. I. Meshcheryakov, A. E. Petrov, K. A. Sarksyan, et al., in *Proceedings of the 41st EPS Conference on Plasma Physics, Berlin, 2014,* Paper P4.053. http://ocs.ciemat.es/EPS2014PAP/pdf/P4.053.pdf.
12. A. I. Meshcheryakov, I. Yu. Vafin, and I. A. Grishina, Plasma Phys. Rep. **46**, 1144 (2020).
13. S. Kubo, H. Takahashi, T. Shimozuma, Y. Yoshimura, M. Nishiura, H. Igami, S. Ogasawara, and R. Makino, EPJ Web Conf. **32**, 02007 (2012).
14. B. Ph. van Milligen, B. A. Carreras, C. Hidalgo, A. Cappa, and TJ-II Team, Phys. Plasmas **25**, 062503 (2018).
15. Yu. N. Dnestrovskij, A. V. Danilov, A. Yu. Dnestrovskij, S. E. Lysenko, A. V. Melnikov, A. R. Nemets, M. R. Nurgaliev, G. F. Subbotin, N. A. Solovev, D. Yu. Sychugov, and S. V. Cherkasov, Plasma Phys. Control. Fusion **63**, 055012 (2021).
16. M. Yu. Kantor, A. J. H. Donné, R. Jaspers, H. J. van der Meiden, and TEXTOR Team, Plasma Phys. Control. Fusion **51**, 055002 (2009).
17. E. Pasch, M. N. A. Beurskens, S. A. Bozhenkov, G. Fuchert, J. Knauer, R. C. Wolf, and W7-X Team, Rev. Sci. Instrum. **87**, 11E729 (2016).
18. A. Krämer-Flecken, X. Han, T. Windisch, J. Cosfeld, P. Drews, G. Fuchert, J. Geiger, O. Grulke, C. Killer, A. Knieps, Y. Liang, S. Liu, M. Rack, and the W7-X team, Plasma Phys. Control. Fusion **61**, 054003 (2019).
19. E. Z. Gusakov and A. Yu. Popov, Phys. Rev. Lett. **105**, 115003 (2010).
20. E. Gusakov and A. Popov, Europhys. Lett. **99**, 15001 (2012).
21. A. Yu. Popov and E. Z. Gusakov, Plasma Phys. Control. Fusion **57**, 025022 (2015).
22. A. Yu. Popov and E. Z. Gusakov, Europhys. Lett. **116**, 45002 (2016).
23. A. Yu. Popov and E. Z. Gusakov, JETP Lett. **105**, 78 (2017).
24. E. Z. Gusakov, A. Yu. Popov, A. N. Saveliev, and E. V. Sysoeva, Plasma Phys. Control. Fusion **59**, 075002 (2017).
25. E. Z. Gusakov and A. Yu. Popov, Phys. Plasmas **25**, 012101 (2018).
26. E. Z. Gusakov, A. Yu. Popov, and M. A. Irzak, J. Exp. Theor. Phys. **123**, 723 (2016).
27. E. Z. Gusakov and A. Yu. Popov, Phys. Plasmas **23**, 082503 (2016).
28. E. Z. Gusakov and A. Yu. Popov, Plasma Phys. Control. Fusion **59**, 025005 (2017).
29. E. Z. Gusakov and A. Yu. Popov, Phys. Plasmas **25**, 082117 (2018).
30. E. Z. Gusakov and A. Yu. Popov, J. Exp. Theor. Phys. **125**, 702 (2017).
31. E. Z. Gusakov, A. Yu. Popov, and A. N. Saveliev, Phys. Plasmas **25**, 062106 (2018).
32. E. Z. Gusakov and A. Yu. Popov, Plasma Phys. Control. Fusion **60**, 025001 (2018).
33. E. Z. Gusakov and A. Yu. Popov, Nucl. Fusion **59**, 104003 (2019).
34. E. Z. Gusakov and A. Yu. Popov, Plasma Phys. Control. Fusion **62**, 025028 (2020).
35. E. Z. Gusakov and A. Yu. Popov, Nucl. Fusion **60**, 076018 (2020).
36. E. Z. Gusakov and A. Yu. Popov, Phys.-Usp. **63**, 365 (2020).
37. A. B. Altukhov, V. I. Arkhipenko, A. D. Gurchenko, E. Z. Gusakov, A. Yu. Popov, L. V. Simonchik, and M. S. Usachonak, Europhys. Lett. **126**, 15002 (2019).
38. E. Z. Gusakov and A. Yu. Popov, Phys. Plasmas **27**, 082502 (2020).
39. S. K. Hansen, S. K. Nielsen, J. Stober, J. Rasmussen, M. Stejner, M. Hoelzl, T. Jensen, and the ASDEX Upgrade team, Nucl. Fusion **60**, 106008 (2020).
40. A. Tancetti, S. K. Nielsen, J. Rasmussen, D. Moseev, E. Z. Gusakov, A. Yu. Popov, T. Stange, S. Marsen, M. Zanini, C. Killer, M. Vecsei, H. P. Laqua, and W7-X Team, in *Proceedings of the 47th EPS Conference on Plasma Physics, Sitges, 2021,* Paper P4.1048. http://ocs.ciemat.es/EPS2021PAP/pdf/P4.1048.pdf.
41. A. F. Alexandrov, L. S. Bogdankevich, and A. A. Rukhadze, *Principles of Plasma Electrodynamics* (Vysshaya Shkola, Moscow, 1988; Springer-Verlag, Berlin, 1984).
42. E. Z. Gusakov, A. Yu. Popov, and P. V. Tretinnikov, Plasma Phys. Control. Fusion **61**, 085008 (2019).

Translated by I. Grishina